# IDENTIFYING TIME PATTERNS AT THE FIELD SCALE FOR RETRIEVING SUPERFICIAL SOIL MOISTURE ON AN AGRICULTURAL AREA WITH A CHANGE DETECTION METHOD: A PRELIMINARY ANALYSIS

G. Graldi[1,*], A. Vitti[1]

[1] Dept of Civil, Environmental and Mechanical Engineering, University of Trento, Italy - (giulia.graldi, alfonso.vitti)@unitn.it

**Commission III, WG 10**

**KEY WORDS:** Soil moisture, Sentinel-1, field scale, SAR based vegetation index.

**ABSTRACT:**

A preliminary analysis based on the application of a change detection method for remote sensed soil moisture retrieval at high resolution is presented. Sentinel-1 SAR images are used for studying agricultural areas in Spain, where in situ soil moisture data are available through the International Soil Moisture Network. The total backscattered SAR signal is modelled as the sum of vegetation and soil contributions. At first, the relationship between soil moisture and the co-polarized band of Sentinel-1 was analyzed for all the measurement stations of the area, and the ones with stronger relation were selected. Time series analyses were then conducted at the field scale for studying the interactions between some SAR parameters and the in situ data. The two polarizations and the polarization ratio were analyzed with respect to in situ soil moisture observations and precipitation data in order to identify homogeneous time domains in which the method can be applied in a consistent manner. Analyses show that the main driver of wide range SAR signal variations is the presence of precipitation events. Moreover, SAR coherence and polarization rate manifest specific behaviors that can be exploited either for deepening the knowledge on the role of model parameters and identifying suitable time and space extends in which operate separate estimations of vegetation, soil moisture and soil roughness parameters. Identification and isolation of precipitation driven patterns, as long as the selection of homogeneous time spans and space regions is the basis for improving the capability of satellite based soil moisture retrieval models.

## 1. INTRODUCTION

One of the fundamental hydro-climate variables driving the exchanges of water and heat between land and atmosphere is soil moisture. For this reason, from 2010 it is in the list of the Essential Climate Variables to be monitored globally according to the Global Climate Observation System (GCOS, 2010). Spatial information on soil moisture could be indeed useful for a lot of environmental applications such as weather forecasts, monitoring of river basins, management of agricultural practises where coupled with local meteorological forecasting ti can help in optimizing the consumption of water resource.

Information about soil moisture can be obtained at different resolutions and spatial extents by exploiting microwave remote sensing. The microwave signal is indeed sensitive to the dielectric properties of the target superficial layer. Passive microwave imagery are generally used for producing global soil moisture maps characterized by coarse resolutions. The SMOS (Soil Moisture and Ocean Salinity) mission of the European Space Agency (ESA), for example, provide global soil moisture products characterized by resolutions of 25 km and 15 km, and continental products with resolution up to 1 km over Europe and Mediterranean areas (M. Pablos, 2020). Active microwave imaging can instead be exploited for estimating soil moisture at higher resolution. The newest missions carrying Synthetic Aperture Radar (SAR) sensors are indeed capable of acquiring images at resolutions up to a few meters, such as the ESA Sentinel-1 mission (20 m) and the commercial mission ICEYE (3 m).

When working with SAR images on agricultural areas, the active SAR signal coming back from the vegetated surface can be modelled as the sum of the contributions of vegetation and soil. In order to estimate the variations of SAR signal caused by changes in the soil moisture conditions with a Change Detection (CD) method, it is necessary to identify space and time domains in which the variations other contributions could be considered as negligible, so that the CD method can be accurately applied.

Vegetation contribution has been largely modelled by means of optical vegetation indices such as NDVI for the retrieval of superficial soil moisture (Qiu et al., 2019), however optical derived information are not always available due to their dependence from cloud cover conditions and diurnal cycles. As a matter of fact, in the last few years many authors found out that the evolution of the vegetation, and in particular of agricultural crops, can be well described by SAR based vegetation indices (Veloso et al., 2017; Vreugdenhil et al., 2018), thanks to the sensitivity of SAR cross-polarized band to the development of the canopy layer. Also the interferometric coherence was found to be sensitive to the vegetation and consistent with the optical index NDVI, e.g. as shown by Bai et al. (2020). Moreover, SAR based indices have been already used for soil moisture estimation purposes (Ouaadi et al., 2020).

Soil contribution is instead described by two components, namely soil moisture and soil roughness. Giving the lack of information for estimating these two components simultaneously from SAR data (Zribi et al., 2014), usually the influence of soil roughness need to be considered constant in time while retrieving superficial soil moisture. This hypothesis is only valid when the data are elaborated at not very high resolutions, so that the residual effects of changes in soil roughness on the SAR signal are smoothed out (e.g. Gao et al. (2017)). When working on agricultural areas at high resolution, the variations of soil rough-

* Corresponding author

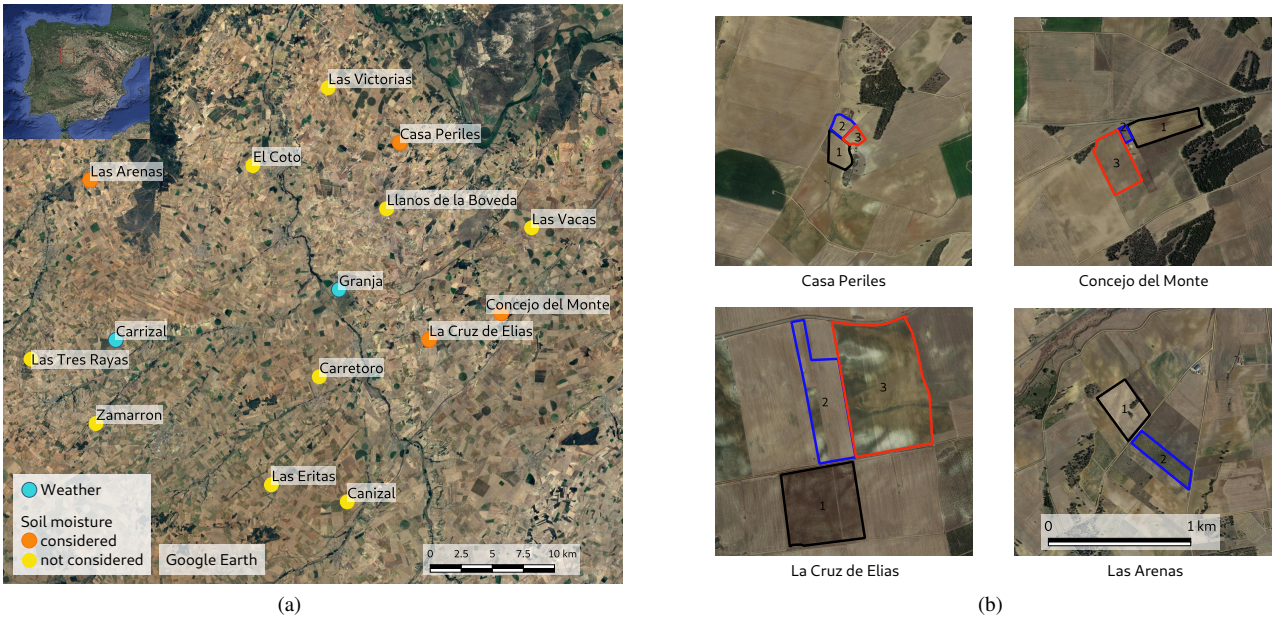


Figure 1. 1a) Location of the study area and of the soil moisture (yelow and orange dots) and weather (light blue dots) stations of the REMEDHUS network. 1b) Selected fields around the measurement stations highlighted in orange in Figure 1a (Casa Periles, Concejo del Monte, La Cruz de Elias and Las Arenas). The fields numbered as 1 present a black outline, fields 2 a blue outline, fields 3 a red outline. Background image of Google Earth under their terms of service.

ness caused by agricultural practises, such as tillage, could not be neglected since they influence the intensity of co-polarized bands.

In the present work a preliminary analysis for estimating superficial soil moisture by means of a change detection method is presented. Specifically, the relationship between the co-polarized VV band of the Sentinel-1 and the daily soil moisture is analyzed, and the time series of the co-polarized band VV, the cross-polarized band VH, a SAR based vegetation index and in situ data are investigated. The study is conducted at the field scale on an agricultural area in Spain for the agricultural season of the year 2020. The time domain is examined by conducting the analysis on a few controlled areas (single crop fields) for which superficial soil moisture measurements and precipitation data are available through the International Soil Moisture Network (ISMN). The analysis is performed only on low vegetated areas, selected by means of the Corine Land Cover 2018 classes of arable land and pastures (2.1 and 2.3).

The present work is composed as follows: the study area and the data used for the elaborations are presented in Section 2; the method with which the analyses are performed is illustrated in Section 3; results are presented and discussed in Section 4; finally, the conclusions are drawn in Section 5.

## 2. MATERIALS

### 2.1 Study case and in situ data

The area of interest is in the Duero river basin in Spain, between the cities of Zamora, Valladolid and Salamanca. For this area are available soil moisture data of the monitoring network REMEDHUS, operated by the Centro Hispano Luso de Investigaciones Agrarias of the University of Salamanca (Martínez-Fernández and Ceballos, 2005). The data of the network are available through the services supplied by the ISMN (Dorigo et al., 2011), providing hourly measurements in $m^3/m^3$ referred to the first 5 cm of the soil surface layer. For the analyses were initially considered 12 stations out of 24 of the network, whose spatial distribution on the study area can be seen in Figure 1 (yellow and orange dots). The selected stations are characterized by low vegetated rainfed crops according to the Corine Land Cover 2018 classification (classes 2.1 and 2.3) and availability of data for the agricultural season of 2020. Precipitation data of two meteorological stations included in the REMEDHUS network were used to analyze the soil moisture time series nearby the selected stations. The position of the weather stations on the study area are reported in light blue in Figure 1.

### 2.2 Sentinel-1 SAR data

SAR images of the Sentinel-1 mission of ESA were used for the analysis. Specifically, 34 GRD (Ground Range Detected) products acquired in the Interferometric Wide-Swath mode were used. The selected data are characterized by the same relative orbit n° 154 and were acquired from both the satellites Sentinel-1A and Sentinel-1B. The data were downloaded using the ONDA API services (ONDA, 2018) and preprocessed with the Sentinel Application Toolbox (SNAP) (ESA, 2019) for obtaining the maps of the backscattering coefficient $\gamma_0$ at the resolution of 20 m for both the VV and VH polarizations. The flow of the preprocessing operations performed is similar to the one suggested by Filipponi (2019). The terrain radiometric correction (Small, 2011) and the geometric correction were applied by using the Digital Elevation Model at 5 m resolution provided from the Spanish National Centre of Geographic Information.

## 3. METHOD

### 3.1 Selection of sites with a high relation between SAR signal and soil moisture

At first, a selection of the sites characterized by a higher sensitivity of the SAR signal with respect to superficial soil moisture was performed. The relationship between some SAR parameters and the measured soil moisture was analyzed for the 12 stations of the REMEDHUS network characterized by low vegetation.
The SAR parameters considered are $\gamma_0^{VV}$, $\gamma_0^{VH}$ and a SAR based vegetation index, called Polarization Ratio (PR), which is the ratio between the cross-polarized and the co-polarized bands. The Radar Vegetation Index (RVI in Equation 1) adjusted on Sentinel-1 data (Trudel et al., 2012) was also tested, but it was found almost equal to PR since the contribution of the co-polarized VV band is dominant in respect to VH, and its results are thus not reported in the following section.

$$RVI = \frac{4\gamma_0^{VH}}{\gamma_0^{VH} + \gamma_0^{VV}} \tag{1}$$

For every station, the SAR parameters were plotted as a function of the daily mean of the measured soil moisture. The parameters of a first order polynomial fitting and determination coefficient $R^2$ were then calculated. The stations with higher $R^2$ were selected for continuing the analysis. Since the SAR backscattered signal of one pixel is characterized by oscillation of intensity due to residual noise left by the preprocessing operations, the analysis were based on the average of SAR parameters over the 9 pixel around the measurement station.

### 3.2 Analyses at the field scale

Since the selected measurement stations are not positioned inside the agricultural fields but at their borders, it is necessary to identify the fields around the measurement points on whose perform the analysis. In Figure 1 the identified fields around the measurement stations are shown together with their reference stations. A time series analysis of the SAR parameters was then conducted for every site in order to study and compare the trends of the SAR parameters in the different fields associated to one measurement stations. After that, for all the fields, the relationships between all the SAR parameters and the observed superficial soil moisture were analyzed, as previously described in 3.1. In the following, the relationships between SAR parameters and in situ measurements are reported and discussed for a set of fields characterized by high values of the determination coefficient.

## 4. RESULTS AND DISCUSSION

After the analysis described in section 3.1, four sites presenting high values of determination coefficient were selected for being further analyzed. Their names are Casa Periles, Concejo del Monte, La Cruz de Elias and Las Arenas and are highlighted in orange in Figure 1. The following results are relative to these four sites.

### 4.1 Working at the field scale: how time series of SAR parameters vary

In Figure 2 and 3 are reported the time series of the average over each field of the SAR parameters for the three fields around

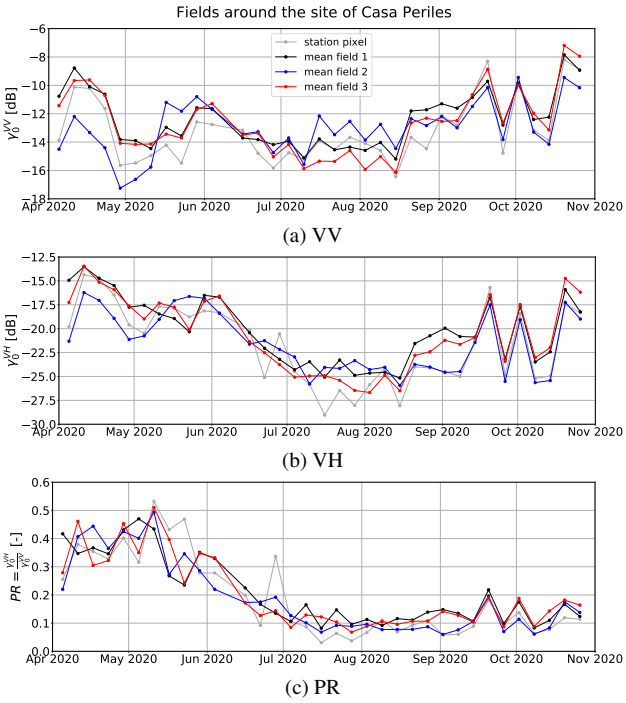


(a) VV

(b) VH

(c) PR

Figure 2. Time series of mean SAR parameters over three fields around the station of Casa Periles. The time series from April to October 2020 of $\gamma_0^{VV}$ in dB, $\gamma_0^{VH}$ in dB and PR are shown respectively in Figure 2a, 2b and 2c. In the graphs the grey line represents the pixel in which lays the measurement station, the black line illustrates the field 1, the blue line the field 2, and the red line the field 3.

the stations of Casa Periles and La Cruz de Elias. These two sites were selected because they present different patterns in between the fields of the same site. Specifically, for the site of Casa Periles (Figure 2) the time series of the SAR parameters are similar for all the three fields, while for the plots of La Cruz de Elias differences in between the fields can be observed (Figure 3). In the plots the grey lines represent the values of the parameters of the pixel in which the measurement station is positioned. The black, blue and red lines represent instead the average of the parameters over a single field that is number 1, 2 and 3 respectively (see Figure 1).
The average values of $\gamma_0^{VV}$ and $\gamma_0^{VH}$ for the fields of Casa Periles (Figures 2a, 2b) exhibit similar patterns. In middle April 2020, they present a peak assuming lower values of intensity for the field 2. At the end of May all the fields display another peak, which starts two epochs in advance for the field 2. From mid July to mid August the three fields assume different values of $\gamma_0^{VV}$ and $\gamma_0^{VH}$, and these differences are wider in the co-polarized band. Finally, the values assumed until the end of the agricultural season are almost equal for the three fields, presenting big oscillations of intensity from mid September to November. Regarding the SAR vegetation index PR, the fields of Casa Periles show the same trend, as can be seen in Figure 2c. Until June 2020, the values of PR present a peak with values going from 0.2 to 0.5, while the index slowly decreases and remain constant during all the rest of the agricultural season. For this site, the values in correspondence of the station pixel (grey line) follow the trend of the fields for all the parameters presenting also some peaks.
For the site of La Cruz de Elias, between the trends of $\gamma_0^{VV}$ and $\gamma_0^{VH}$ in Figure 3a and 3b can be observed similarities for

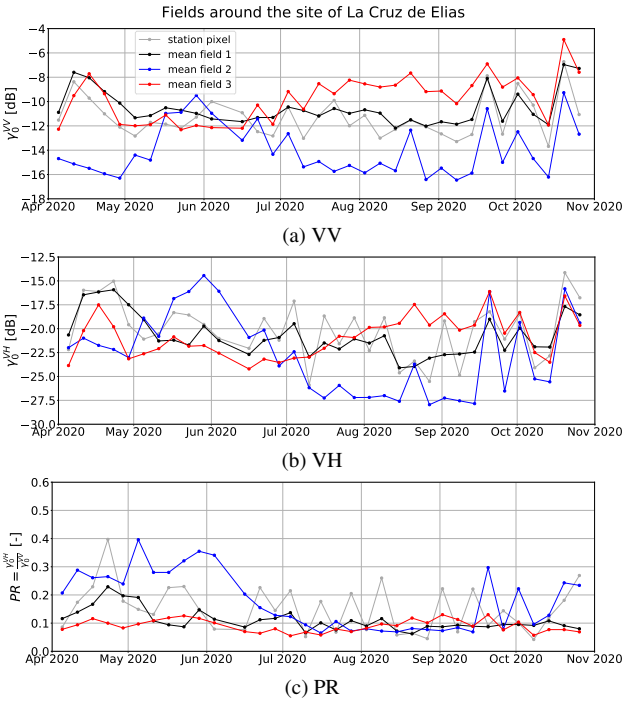


(a) VV

(b) VH

(c) PR

Figure 3. Time series of mean SAR parameters over three fields around the station of La Cruz de Elias. The time series from April to October 2020 of $\gamma_0^{VV}$ in dB, $\gamma_0^{VH}$ in dB and PR are shown respectively in Figure 2a, 2b and 2c. In the graphs the grey line shows the pixel in which lays the measurement station, the black line depicts the field 1, the blue line the field 2, and the red line the field 3.

every field. In general, the cross-polarized band VH presents a wider range of values than that of band VV, but the trends are comparable. Fields 1 and 3 present a peak in April 2020, then from May to June they assume similar values, and finally from June to September they show up different behaviours. Field 2 presents a peak at the end of May 2020 followed by values lower than those of other fields, instead. At the end of the agricultural season, field 2 displays some peaks that can be found also in the fields 1 and 3. The PR index assume different values for the three fields until July, the differences are particularly evident for field 2. This is mainly due to the different values assumed by the VV and VH polarizations for the field 2. From July to September, all the plots assume similar values, while in the last months of the season field 2 presents peak that for the other two fields are present only in the time series of the two polarization. For this site, the $\gamma_0^{VV}$ and $\gamma_0^{VH}$ time series of the station pixel are similar to the ones of the field 1, while the PR presents a lot of peaks and seems not to follow any of the studied fields.

### 4.2 Analysis of intensity based SAR parameters

**4.2.1 Relation in between the intensity based parameter and the superficial soil moisture.** In Figure 4 are reported the plots showing the relation between SAR parameters and measured soil moisture for two fields of interest out of the eleven under analyses. The fields for which results are described below are the field 1 (La Cruz de Elias) and field 1 (Las Arenas), respectively displayed in Figure 4a and 4b. These fields were selected because they present the higher values of $R^2$ for $\gamma_0^{VV}$, equal to 0.589 and 0.599 respectively for La Cruz de Elias and Las Arenas. The values of the determination coefficients are particularly high considering the complex context in which they rose. In fact, when the analysis is performed at high resolution like in the present work, it is challenging to distinguish the influence of the various factors such as the vegetation, the soil roughness and the soil moisture on the backscattered signal. Furthermore, all the other fields under analysis present much lower values of the determination coefficient.
For both the fields, in Figures 4a and 4b it can be observed that $\gamma_0^{VV}$ has a stronger relation with the soil moisture if compared to the other SAR parameters. For both the fields the vegetation index PR instead presents particularly low relation with the superficial soil moisture, with almost null values of the slope $\alpha$ of the fitting first order polynomial. From these plots, one can observe that PR is not correlated with the the values of the measured soil moisture. This means that it could be used for modelling the vegetation contribution without introducing a strong dependence on the soil moisture content.
Finally, the distribution of the two samples showed in Figure 4 don't cluster as a function of time for any of the SAR parameters. Other fields and sites of the study area presented time-related grouping suggesting a seasonal relationship (herein not reported for the sake of brevity).

**4.2.2 Time series of intensity based SAR parameters and in situ measurements.** For the two selected fields, in Figure 5 and 6 are reported the time series of the SAR parameters and the in situ measured data. Specifically, the blue line represents $\gamma_0^{VV}$, the red line $\gamma_o^{VH}$ and the green line the vegetation index PR, while for the in situ data the measured soil moisture is displayed with a light blue line and the precipitation with grey bars. Since the values of the SAR parameters in the plots are the average over the field, information about the intra-filed spatial variation of the parameters is provided by the standard deviation represented in the plots by means of color-shadowed backgrounds of the corresponding average values.
For both fields, the polarizations present similar trends in some intervals of the study period. For La Cruz de Elias (Figure 5) $\gamma_0^{VV}$ and $\gamma_0^{VH}$ display a peak in April 2020, when also the soil moisture presents some peaks in correspondence of precipitation events. Three peaks are also depicted in September, October and November in correspondence of precipitation events and soil moisture peaks. Similar peaks in $\gamma_0^{VV}$ , $\gamma_0^{VH}$, soil moisture and precipitations can be seen on the graphs of Figure 6 for the field of Las Areans. All the trends above described have in common the occurrence of some precipitation event, yielding consequent increases of the soil moisture content and the intensity values of both polarizations.
The time series of $\gamma_0^{VH}$ in La Cruz de Elias in Figure 5 presents peaks also not in correspondence of precipitation events during the middle of the agricultural season, from late May until mid August 2020. Similar peaks during July and August are present in the cross-polarized band for the field of Las Arenas (Figure 6).
The time series of the PR index for the field of La Cruz de Elias (Figure 5) is influenced by the peaks of the VH band taking place in April and in the middle of the agricultural season. From the end of August instead, the index can be considered as almost constant. In the field of Las Arenas (Figure 5), the PR index is more stable during the first part of the agricultural season, until half June. Then it presents peaks like the ones exhibit by $\gamma_0^{VH}$ in July and during the precipitation events of September and October.

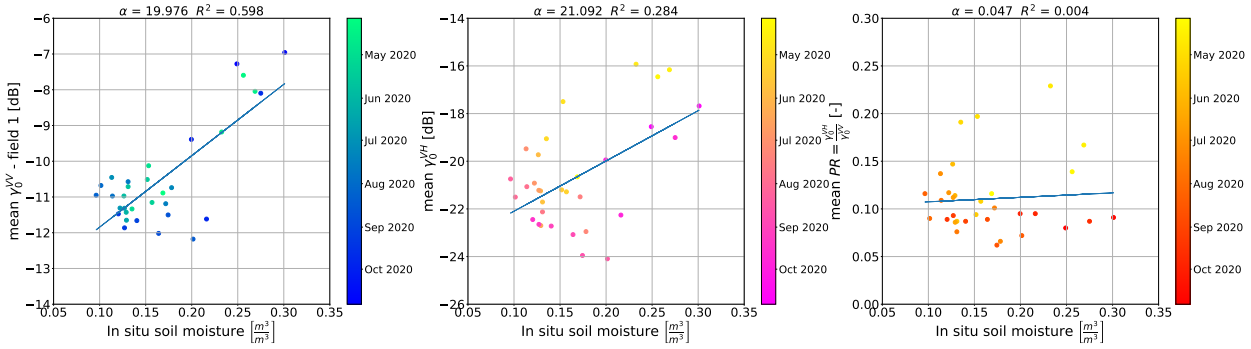


(a) La Cruz de Elias

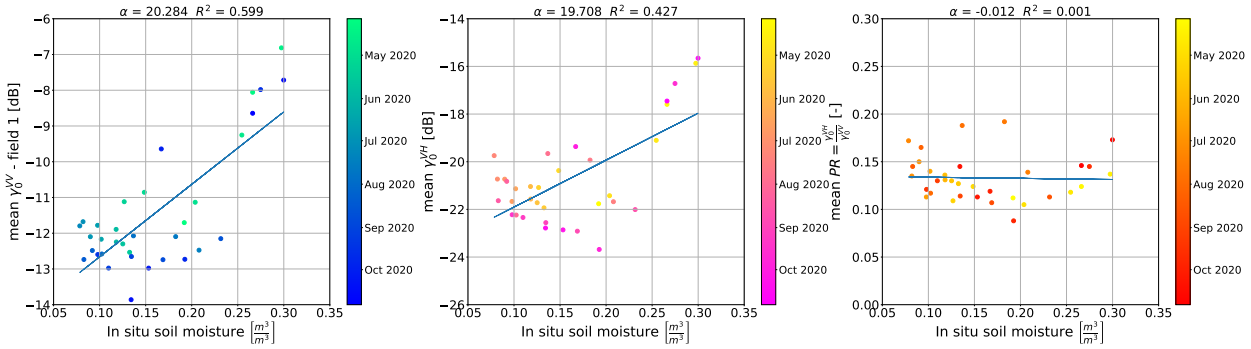


(b) Las Arenas

Figure 4. Comparison between superficial soil moisture in $m^3/m^3$ and SAR parameters for the field 1 of 4a) La Cruz de Elias and 4b) Las Arenas. For all the SAR parameters $\gamma_0^{VV}$ in dB, $\gamma_0^{VH}$ in dB and PR are reported the slope $\alpha$ of the fitting straight line and the coefficient of determination $R^2$.

**4.2.3 Impact of the occurrence of precipitation events in the relation between $\gamma_0^{VV}$ and soil moisture.** Given the increase of $\gamma_0^{VV}$ values in correspondence of precipitation events observed in the two fields under analysis, the overlapping dates are identified and highlighted in red in the graph showing the relations between $\gamma_0^{VV}$ and the measured soil moisture. The results are reported in Figure 7a and 7b for La Cruz de Elia and Las Arenas. For both the fields, the selected dates shape a cluster characterized by high values of soil moisture and $\gamma_0^{VV}$. The points of the sample not linked to precipitation events group themselves in between values characterized by small variations of $\gamma_0^{VV}$ and of soil moisture suggesting the need to investigate more on these point set in order to identify other driving factors of backscattered signal once excluded the strong precipitation influence.

### 4.3 VH interferometric coherence versus VV and VH intensities

Since the SAR backscattered signal in both polarizations showed a dependence on precipitations, another satellite parameter based on the SAR phase information was tested. The coherence of the VH band $\rho^{VH}$ was calculated from SLC (Single Look Complex) data of Sentinel-1. In the following, the relations between $\rho^{VH}$ and the differences of $\gamma_0^{VV}$ and $\gamma_0^{VH}$ for all pixels of field 1, La Cruz de Elias, are illustrated in Figure 8. In the x-axis are reported the differences of intensity between the dates of 11/04/2020 and 23/04/2020, while in the y-axis the coherence values between the two days are displayed. For both VV (Figure 8a) and VH (Figure 8b), the values of intensity have a wider range of variation in respect to the values assumed by the coherence, concentrated around one. Given that $\rho^{VH}$ values almost equal to one indicate that no changes have occurred in the phase information, the coherence seems more stable in respect to the intensity of $\gamma_0^{VV}$ and $\gamma_0^{VH}$ between the two considered days.
In Figure 9 it is finally reported a false color image where $\gamma_0^{VH}$ of the first epoch is used as red channel, $\gamma_0^{VH}$ of the second epoch is used as green channel and the coherence between the two epochs is used as blue channel. When the image assumes yellow values it means that the coherence presents low values, and that the $\gamma_0^{VH}$ values of the two dates contribute with a similar intensity, and so that they remain constant over the two dates. Where instead prevail blue and purple the coherence values are high and predominant.

## 5. CONCLUSIONS

The differences that can be observed in the time series of the different fields around a single station and in between different sites, showed how rich is the variation of the SAR response on an agricultural area. In particular, it is interesting to note that not only the cross-polarized band, which is sensitive to the presence and type of vegetation, vary from field to field, but also the co-polarized VV band which is instead more linked to the properties of the soil. Given these variations in both the polarizations, the availability of in situ measurement of soil moisture inside a single field and not on field borders would be more useful for individuating locally the effect on the SAR signal of the different contributing factors, such as vegetation and soil moisture changes, and eventually soil roughness.
This study concentrated on fields showing high values of determination coefficient for the linear fitting of SAR parameters and in situ soil moisture observations. It is essentially easier to start the investigation and the modelling of SAR-based retrieval of soil moisture at the field scale in study areas of this kind.

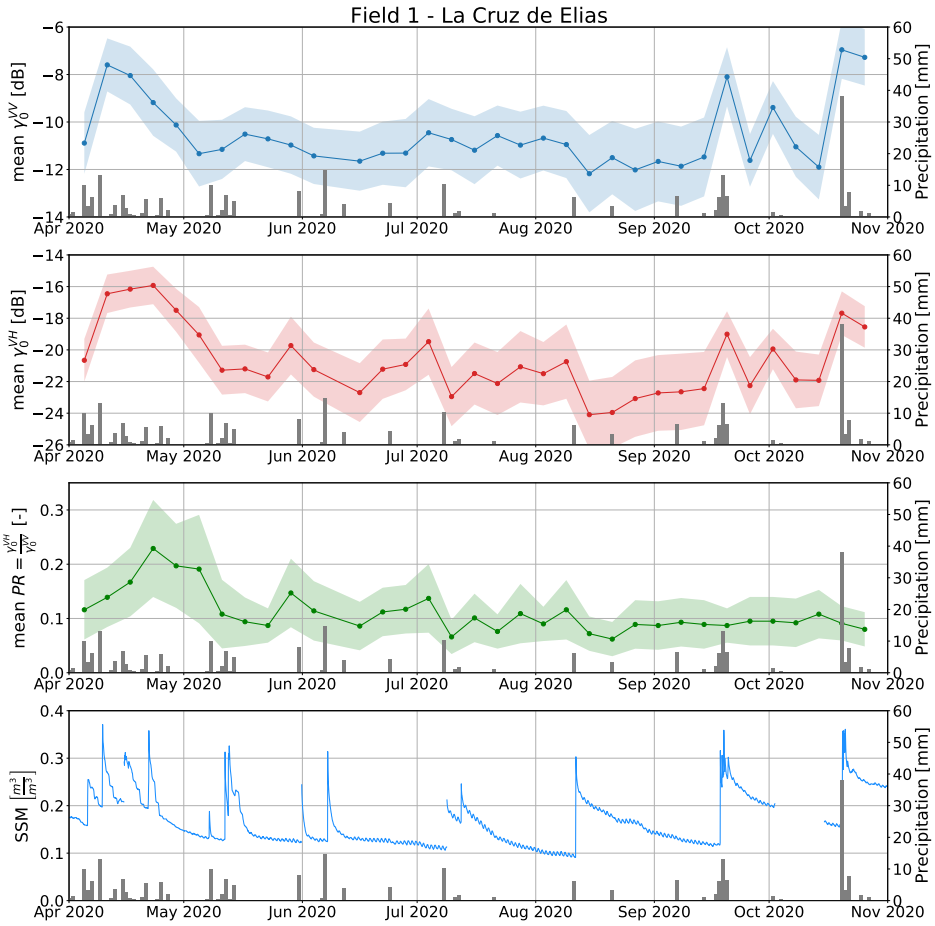


Figure 5. Time series of mean SAR parameters over field 1 of La Cruz de Elias and in situ data registered from the stations. The time series from April to October 2020 is reported. $\gamma_0^{VV}$ in dB is represented in blue, $\gamma_0^{VH}$ in dB is illustrated in red, PR is described with a green line, in situ soil moisture in $m^3/m^3$ are shown with a light blue line and finally, the precipitations in mm are reported with gray bars. The shadows in the SAR parameters graphs represent the standard deviation over the field 1 for every date.

However, the knowledge advance gained in these cases would guide methodological adaptations and improvements which are needed to tackle more complex situations in which the contributions and interactions of the considered model parameters are much more diversified and challenging.

For the fields showing higher relationships between the co-polarized band and the measured soil moisture, our analysis suggested that this relation is mainly driven by the occurrence of precipitation events. In the examples here reported, the values of both $\gamma_0^{VV}$ and $\gamma_0^{VH}$ increase in presence of precipitations. Oscillations of the intensity values in correspondence of precipitation events have been studied both for marine (Danklmayer and Chandra, 2009) and land (Khabbazan et al., 2022) applications. The physical phenomenon behind this increase on agricultural fields cannot be addressed in the present work. To deepen the analysis about the clustering showed in Figure 7a and 7b after the removal of precipitation driven values, much more field data is required. Accurate knowledge of agriculture and irrigation practices as long as vegetation and crop phases are necessary for tackling the modelling of those parameters on the time series of SAR based observations.

## 6. ACKNOWLEDGMENTS

For this work were used Copernicus Service information 2022 and modified Copernicus Sentinel data 2020. The authors would also thank the Reaserch Group of Water Resources of the University of Salamanca (Spain) for providing data to support this study.

## References

Bai, Z., Fang, S., Gao, J., Zhang, Y., Jin, G., Wang, S., Zhu, Y., Xu, J., 2020. Could Vegetation Index be Derive from Synthetic Aperture Radar? – The Linear Relationship between Interferometric Coherence and NDVI. *Scientific Reports*, 10(1).

Danklmayer, A., Chandra, M., 2009. Precipitation induced signatures in SAR images. *3rd European Conference on Antennas and Propagation*.

Dorigo, W. A., Wagner, W., Hohensinn, R., Hahn, S., Paulik, C., Xaver, A., Gruber, A., Drusch, M., Mecklenburg, S., van Oevelen, P., Robock, A., Jackson, T., 2011. The International Soil Moisture Network: a data hosting facility for global in situ soil moisture measurements. *Hydrology and Earth System Sciences*, 15(5), 1675–1698.

ESA, 2019. Snap - esa sentinel application platform v7.

Filipponi, F., 2019. Sentinel-1 GRD Preprocessing Workflow. *Proceedings*, 18(1), 11.

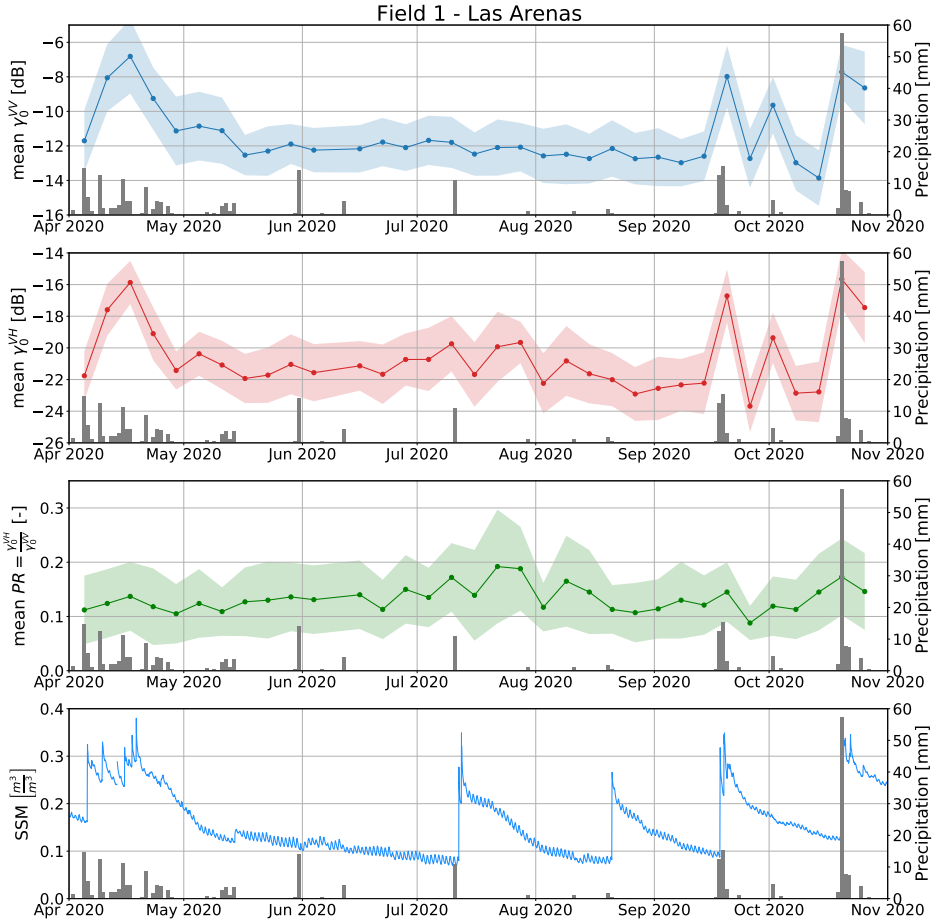


Figure 6. Time series of mean SAR parameters over field 1 of Las Arenas and in situ data registered from the stations. The time series from April to October 2020 is reported. $\gamma_0^{VV}$ in dB is represented in blue, $\gamma_0^{VH}$ in dB is illustrated in red, PR is described with a green line, in situ soil moisture in $m^3/m^3$ are shown with a light blue line and finally, the precipitations in mm are reported with gray bars. The shadows in the SAR parameters graphs represent the standard deviation over the field 1 for every date.

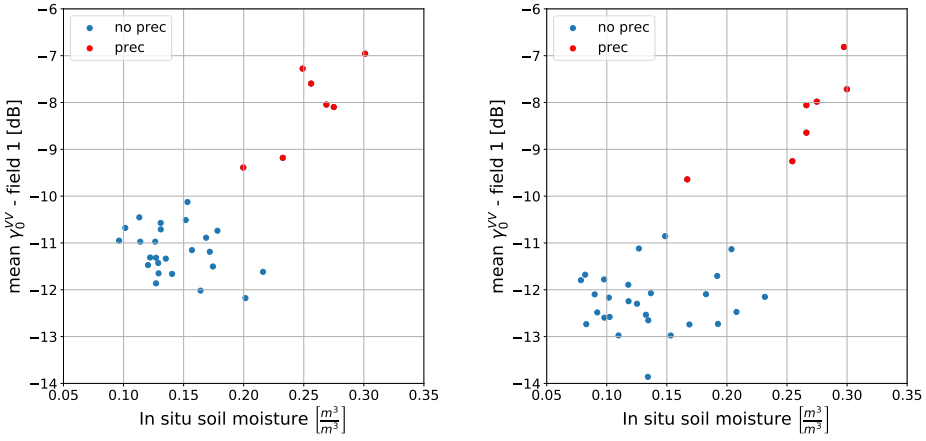


(a) La Cruz de Elias (b) Las Arenas

Figure 7. Comparison between superficial soil moisture in $m^3/m^3$ and $\gamma_0^{VV}$ in dB for the field 1 of 7a) La Cruz de Elias and 7b) Las Arenas, with highlighted in red the dates corresponding to precipitation events.

Gao, Q., Zribi, M., Escorihuela, M., Baghdadi, N., 2017. Synergetic Use of Sentinel-1 and Sentinel-2 Data for Soil Moisture Mapping at 100 m Resolution. *Sensors*, 17(9), 1966.

GCOS, 2010. Implementation plan for the global observing system for climate in support of the unfccc. Technical Report WMO/TD No. 1244. 23pp.

Khabbazan, S., Steele-Dunne, S., Vermunt, P., Judge, J., Vreugdenhil, M., Gao, G., 2022. The influence of surface canopy water on the relationship between L-band backscatter and biophysical variables in agricultural monitoring. *Remote*

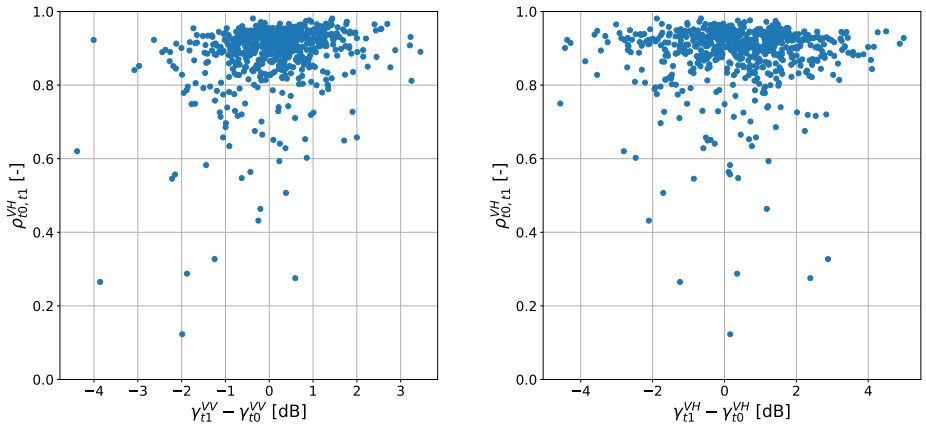


(a) VV (b) VH

Figure 8. Relation between difference of intensity of the two polarizations 8a) VV and 8b) VH and interferometric SAR coherence of the VH polarization $\rho_0$ in between the dates of 11/04/2020 and 23/04/2020 for all the pixel of the field 3 of La Cruz de Elias.

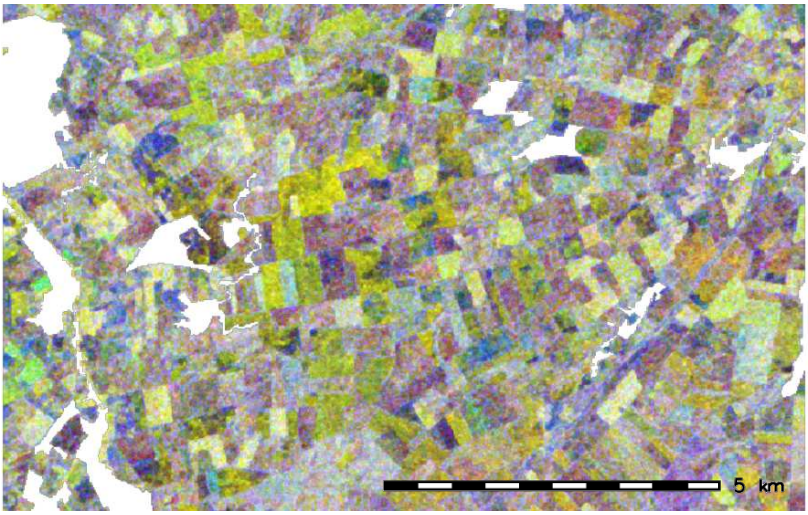


Figure 9. False color image composed by $\gamma_0^{VH}$ in 11/04/2020 in red, $\gamma_0^{VH}$ in 23/04/2020 in green and VH coherence $\rho$ between 11/04/2020 and 23/04/2020 in blue.

*Sensing of Environment*, 268, 112789.

M. Pablos, C. González-Haro, M. P., 2020. Bec smos soil moisture products description. Technical report, Barcelona Expert Centre.

Martínez-Fernández, J., Ceballos, A., 2005. Mean soil moisture estimation using temporal stability analysis. *Journal of Hydrology*, 312(1-4), 28–38.

ONDA, 2018. Onda copernicus data and information access service.

Ouaadi, N., Jarlan, L., Ezzahar, J., Zribi, M., Khabba, S., Bouras, E., Bousbih, S., Frison, P.-L., 2020. Monitoring of wheat crops using the backscattering coefficient and the interferometric coherence derived from Sentinel-1 in semi-arid areas. *Remote Sensing of Environment*, 251, 112050.

Qiu, J., Crow, W. T., Wagner, W., Zhao, T., 2019. Effect of vegetation index choice on soil moisture retrievals via the synergistic use of synthetic aperture radar and optical remote sensing. *International Journal of Applied Earth Observation and Geoinformation*, 80, 47–57.

Small, D., 2011. Flattening Gamma: Radiometric Terrain Correction for SAR Imagery. *IEEE Transactions on Geoscience and Remote Sensing*, 49(8), 3081–3093.

Trudel, M., Charbonneau, F., Leconte, R., 2012. Using RADARSAT-2 polarimetric and ENVISAT-ASAR dual-polarization data for estimating soil moisture over agricultural fields. *Canadian Journal of Remote Sensing*, 38(4), 514-527.

Veloso, A., Mermoz, S., Bouvet, A., Toan, T. L., Planells, M., Dejoux, J.-F., Ceschia, E., 2017. Understanding the temporal behavior of crops using Sentinel-1 and Sentinel-2-like data for agricultural applications. *Remote Sensing of Environment*, 199, 415–426.

Vreugdenhil, M., Wagner, W., Bauer-Marschallinger, B., Pfeil, I., Teubner, I., Rüdiger, C., Strauss, P., 2018. Sensitivity of Sentinel-1 Backscatter to Vegetation Dynamics: An Austrian Case Study. *Remote Sensing*, 10(9), 1396.

Zribi, M., Gorrab, A., Baghdadi, N., 2014. A new soil roughness parameter for the modelling of radar backscattering over bare soil. *Remote Sensing of Environment*, 152, 62–73.